Erythrocyte CD55 facilitates the internalization of *Plasmodium falciparum* parasites

Bikash Shakya[1], Saurabh D. Patel[2], Yoshihiko Tani[3], and Elizabeth S. Egan[1*]

[1]Departments of Pediatrics and Microbiology & Immunology, Stanford University School of Medicine, Stanford, CA 94305, USA

[2]Zuckerman Institute, Columbia University, New York City, NY 10027, USA

[3]Japanese Red Cross Osaka Blood Center, Osaka, Japan

*Correspondence: eegan@stanford.edu

Abstract

Invasion of human erythrocytes by the malaria parasite *Plasmodium falciparum* is a multi-step process. Previously, a forward genetic screen for *P. falciparum* host factors identified erythrocyte CD55 as essential for invasion, but its specific role and how it interfaces with the other factors that mediate this complex process are unknown. Using CRISPR-Cas9 editing, antibody-based inhibition, and live cell imaging, here we show that CD55 is specifically required for parasite internalization. Pre-invasion kinetics, erythrocyte deformability, and echinocytosis were not influenced by CD55, but entry was inhibited when CD55 was blocked or absent. Visualization of parasites attached to CD55-null erythrocytes point to a role for CD55 in progression of the moving junction. Our findings demonstrate that CD55 acts after discharge of the parasite's rhoptry organelles,

and plays a unique role relative to all other invasion receptors. As the requirement for CD55 is strain-transcendent, these results suggest that CD55 or its interacting partners may hold potential as therapeutic targets for malaria.

Key Words

Malaria, CD55, erythrocyte, invasion, *Plasmodium falciparum*

Introduction

Malaria is caused by Apicomplexan parasites of the genus *Plasmodium*, of which *Plasmodium falciparum* is responsible for the majority of severe disease cases in humans. One of the world's major public health problems, malaria causes an estimated 216 million infections and ~445,000 deaths annually, primarily among young children and pregnant women (WHO, 2018). *P. falciparum* has a complex life cycle involving stages in the human and mosquito, but disease only occurs during the blood stage, when parasites infect and replicate in human red blood cells (RBCs). As *P. falciparum* is an obligate intracellular parasite, understanding the molecular determinants of its developmental cycle within RBCs may lead to new therapies. For example, a number of *Plasmodium* proteins that play key roles during erythrocyte invasion have shown promise as vaccine candidates (Ord, Rodriguez, & Lobo, 2015; Sack, Kappe, & Sather, 2017; Salinas, Tang, & Tolia, 2019). Since natural genetic variation in red cells can influence innate susceptibility to malaria, host erythrocyte factors may also hold potential as therapeutic targets (Taylor & Fairhurst, 2014). The identification and study of such factors, however,

46 has been severely limited by the intractability of mature RBCs, which lack a nucleus and
47 DNA.
48
49 *P. falciparum* invasion of erythrocytes involves a series of coordinated events that unfold
50 rapidly over the course of ~2 minutes. These events can be divided into three phases:
51 pre-invasion, active invasion, and echinocytosis (Gilson & Crabb, 2009; Weiss et al.,
52 2015). The process is initiated with the rupture of a "mother" parasite, termed a schizont,
53 which releases up to 32 daughter merozoites. During the pre-invasion phase, a free
54 merozoite makes initial contact with the red cell, stimulating shallow deformation of the
55 host cell plasma membrane. Next, the merozoite reorients so its apically-localized
56 organelles are abutting the cell surface. Reorientation is associated with significant
57 membrane deformation and involves interactions between *P. falciparum* ligands such as
58 the erythrocyte binding antigen (EBA) and reticulocyte binding-like homologues (Rh)
59 family proteins, and receptors on the red cell surface (Gilson & Crabb, 2009; Paul, Egan,
60 & Duraisingh, 2015; Riglar et al., 2011; Tham, Healer, & Cowman, 2012; Weiss et al.,
61 2015). Several ligand and receptor pairs have been shown to act at this stage, often in a
62 strain-specific manner (e.g. PfEBA-175 and GYPA; PfEBA-181 and GYPB PfEBA-140
63 and GYPC; and PfRh4 and CR1), but experimental data suggest their roles in apical
64 reorientation and host cell deformation are largely functionally redundant (Tham et al.,
65 2012).
66
67 The only receptor-ligand interaction known to be essential during the pre-invasion phase
68 involves basigin and PfRH5, which exists in a complex with PfRipr and CyRPA (Chen et

69 al., 2011; Crosnier et al., 2012; Dreyer et al., 2012; Reddy et al., 2015). Binding of the
70 PfRH5 complex to basigin is required for discharge of the rhoptry organelles into the
71 invaded cell and is associated with a calcium spike, potentially due to formation of a pore
72 at the erythrocyte surface (Volz et al., 2016; Weiss et al., 2015). Blocking the interaction
73 between PfRH5 and basigin with specific antibodies prevents invasion (Crosnier et al.,
74 2012).
75
76 Discharge of the rhoptry organelles heralds the start of active invasion. Among the
77 proteins injected from the rhoptries are those of the RON complex (RON 2, RON 4 and
78 RON5), which together form a receptor for binding by the PfAMA1 protein localized on
79 the merozoite surface (Alexander, Arastu-Kapur, Dubremetz, & Boothroyd, 2006;
80 Alexander, Mital, Ward, Bradley, & Boothroyd, 2005; Richard et al., 2010). The interaction
81 between PfAMA1 and the RON complex forms a moving junction between the parasite
82 and host cell that is believed to be entirely parasite-derived (Besteiro, Dubremetz, &
83 Lebrun, 2011; Besteiro, Michelin, Poncet, Dubremetz, & Lebrun, 2009; Harvey, Yap,
84 Gilson, Cowman, & Crabb, 2014; Koch & Baum, 2016). The moving junction provides an
85 anchoring point for the merozoite to actively invade using its own actinomyosin motor;
86 inhibiting the interaction between PfAMA1 and RON prevents invasion (Richard et al.,
87 2010; Srinivasan et al., 2011; Yap et al., 2014).
88
89 As invasion proceeds, a parasitophorous vacuole is formed from components of the host
90 cell membrane and rhoptries, yielding a protective niche for development of the new
91 daughter parasite. The third phase, echinocytosis, is a transient period of cell dehydration

92 and shrinkage observed after invasion; current evidence suggests it is triggered by
93 discharge of the rhoptry contents, prior to and independent of active invasion.
94 Echinocytosis is inhibited by reagents that prevent rhoptry discharge, such as antibodies
95 targeting basigin or PfRH5 (Weiss et al., 2015).
96
97 Most host factors known to play a role in *P. falciparum* invasion have been identified
98 based on their ability to bind to established invasion ligands or from studies of rare natural
99 mutants (Bei & Duraisingh, 2012). Given the inherent intractability of mature RBCs, which
100 lack a nucleus and DNA, the use of genetic approaches to identify and characterize
101 malaria host factors presents a logistical challenge (Egan, 2017). Recently, an shRNA-
102 based forward genetic screen using cultured red cells (cRBCs) derived ex-vivo from
103 primary human hematopoietic stem/progenitor cells (HSPCs) identified erythrocyte CD55
104 (aka DAF) as a critical host factor for *P. falciparum* invasion (Egan et al., 2015). A 70 kD
105 extracellular glycoprotein anchored to the red cell membrane by a
106 glycosylphosphatidylinositol (GPI) linkage, CD55 is broadly distributed in different tissues
107 and secretions, including blood cells (Cooling, 2015; Storry, Reid, & Yazer, 2010). On
108 erythrocytes, CD55 acts as a complement regulatory protein to prevent complement-
109 mediated damage. On epithelial cells, it has been shown to act as a receptor for Group B
110 coxsackie virus and Dr+ E. coli (Cooling, 2015; Coyne & Bergelson, 2006).
111
112 We have shown that *P. falciparum* invasion efficiency was reduced by ~50% in CD55-
113 knockdown cRBCs, and natural CD55-null erythrocytes from two rare donors with the
114 Inab phenotype were resistant to invasion (Egan et al., 2015). Importantly, the

115 requirement for CD55 was strain-transcendent, suggesting that it plays a conserved role
116 in *P. falciparum* invasion. However, the precise function of CD55 during invasion and how
117 it may interface with established ligands or receptors is unknown.
118
119 In this study, we investigated the functional role of CD55 during *P. falciparum* invasion
120 using CRISPR-Cas9 genome editing, antibody-based inhibition and live cell microscopy.
121 We found that CD55 plays a critical role during *P. falciparum* invasion of mature
122 erythrocytes, where it is specifically required for parasite internalization. As a host factor
123 that acts after discharge of the parasite's rhoptry contents, CD55 plays a unique role
124 relative to other receptors required for invasion, providing a crucial link between the
125 ligand-receptor interactions important for adhesion and deformation and effective
126 internalization.
127
128 **Results**
129 **Generation of CD55-null red blood cells using CRISPR-Cas9**
130 Previously, we observed that *P. falciparum* merozoites from several laboratory-adapted
131 strains and clinical isolates displayed impaired invasion into cryopreserved CD55-null
132 RBCs from two rare patients with the Inab phenotype (Egan et al., 2015). To study the
133 requirement for CD55 in an isogenic background, we sought to generate CD55-null
134 cRBCs from HSPCs using CRISPR-Cas9 genome editing by co-delivering single guide
135 RNAs (sgRNAs) and Cas9 in a ribonucleoprotein complex (RNP), a method that has been
136 used previously to generate null mutants in primary human CD34+ cells (Hendel et al.,
137 2015). We designed two chemically modified sgRNAs targeting the 5' end of *CD55*, and

138 delivered them individually or together into primary human $CD34^+$ HSPCs via
139 nucleofection, in complex with recombinant Cas9 (Fig. 1 A). As a control, isogenic $CD34^+$
140 HSPCs from the same donor were nucleofected with Cas9 alone. After inducing the cells
141 to differentiate down the erythroid lineage for 18 days, we observed a high percentage of
142 CD55-null cRBCs in the RNP-transfected populations; a single sgRNA targeting exon 1
143 resulted in ~70% CD55-null cRBCs, while the combination of two sgRNAs targeting exons
144 1 and 2 increased the knockout efficiency to ~90% (Figure 1B). The cells proliferated ~
145 10,000-fold and the enucleation rate was >90% in both the CD55-null cells and wild-type
146 controls, demonstrating that the progenitors differentiated efficiently and that CD55 is not
147 required for this process (Figure S1). The absence of CD55 expression in the mutant
148 cRBCs was also confirmed using immunofluorescence assays (Figure S2).
149

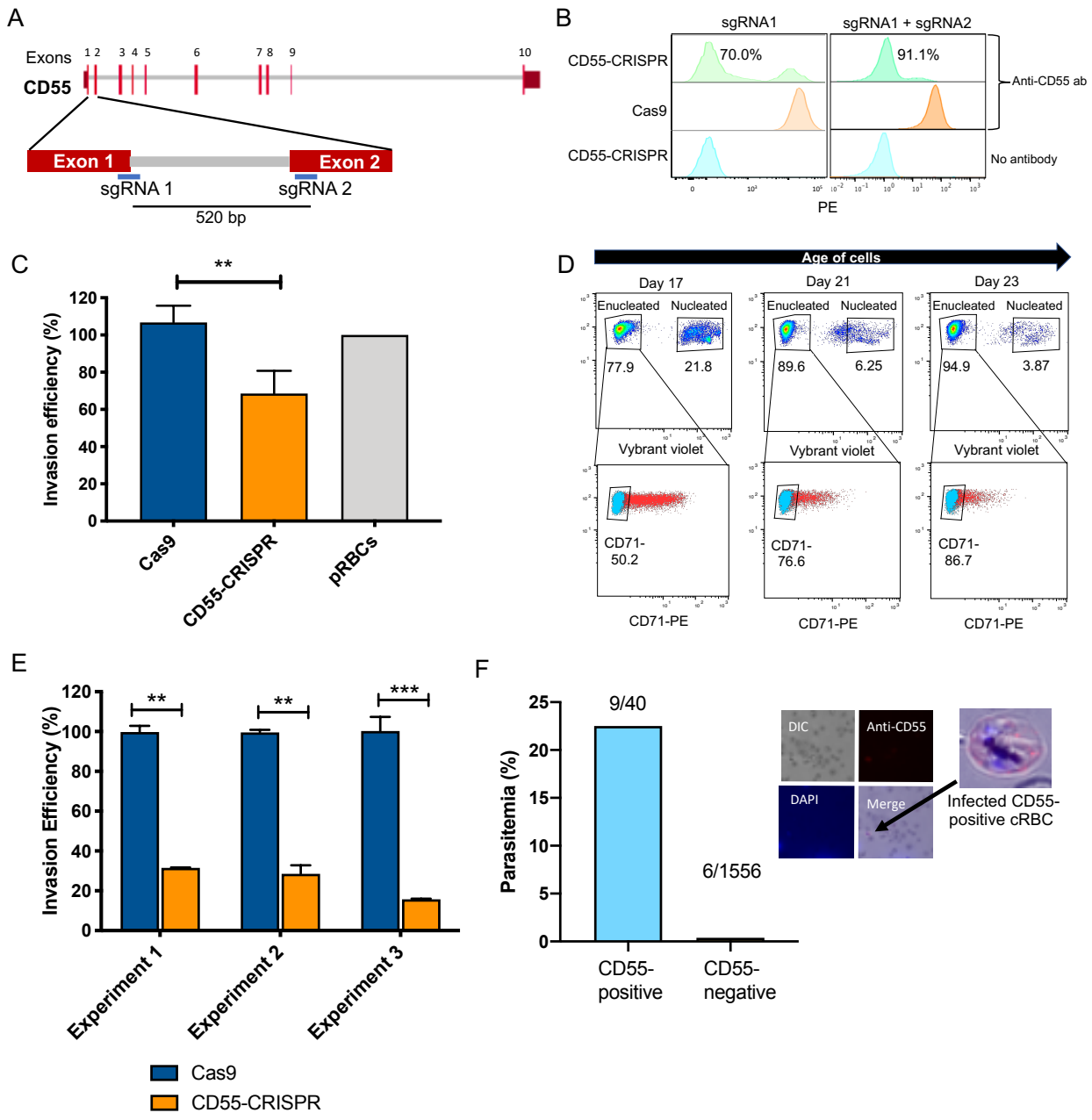

Figure 1: CD55 is required for *P. falciparum* invasion (A) Schematic of *CD55* gene structure showing targeting sites of two single guide RNAs (sgRNAs). Vertical red lines indicate the positions of *CD55* exons. (B) Expression of CD55 on mutant (CD55-CRISPR) cRBCs generated with one sgRNA (left) or two sgRNAs (right), as compared to control (Cas9) cRBCs. (C) Invasion efficiency of *P. falciparum* 3D7 in Day 18 CD55-CRISPR cRBCs compared to isogenic controls (Cas9), relative to the invasion efficiency in peripheral blood erythrocytes (N=4 biological replicates; n=3 technical replicates; error bars indicate SEM; **p<0.01). (D) Time course of expression of CD71 on cRBCs harvested on different days of differentiation. Enucleated versus nucleated cells were gated using a nuclear dye. (E) Invasion efficiency of *P. falciparum* strain 3D7 in CD71-negative, CD55-CRISPR cRBCs compared to CD71-negative isogenic controls (Cas9). Invasion

efficiency is presented relative to the mean of Cas9 control. Three independent biological replicates are shown; error bars represent SEM (n=2 or 3 technical replicates; **$p<0.01$, ***$p<0.005$). (F) Parasitemia in population of CD55-CRISPR cRBCs, in which ~90% of the cells lack CD55 (CD55-negative), and the remaining are CD55-positive, as quantified by immunofluorescence assays. Below are representative images of CD55-CRISPR cRBCs infected with *P. falciparum*. Images are brightfield with fluorescence overlaid. Blue, dapi. Red, anti-CD55-PE.

167 **CD55 is required for *P. falciparum* invasion**

168 To specifically assess the requirement for CD55 for *P. falciparum* invasion, we performed
169 invasion assays using strain 3D7 in CD55-CRISPR cRBCs or in isogenic control cRBCs
170 that had been differentiated for 18 days. While invasion into the CD55-CRISPR cRBCs
171 was impaired relative to the control cells, it was only reduced by ~40% (Figure 1C). This
172 subtle phenotype was reminiscent of the results for CD55-knockdown cRBCs, and
173 differed from the strong invasion phenotype observed in erythrocytes from two CD55-null
174 patients (Egan et al., 2015). Since cRBCs are less mature than erythrocytes from
175 peripheral blood, we hypothesized that the relatively mild invasion phenotype observed
176 in the CD55-null cRBCs may be explained by the overall maturation state of the ex-vivo
177 cultures on day 18.

178

179 To begin to determine whether cell maturity modifies the requirement for CD55 during *P.*
180 *falciparum* invasion, we assessed the surface expression of CD71 in the cRBCs, which
181 is highly expressed on erythroblasts and young reticulocytes, but quickly disappears as
182 reticulocytes mature into erythrocytes (J. Hu et al., 2013). Flow cytometry on day 17
183 demonstrated that approximately 50% of the enucleated cRBCs were CD71-positive and
184 ~50% were CD71 negative, indicating a mix of cell maturity in the population (Figure 1D).
185 This was further validated using a reticulocyte stain (Figure S3), which showed that day
186 17 cells were ~ 50% reticulocytes and 50% erythrocytes. A timecourse over 7 additional
187 days of terminal differentiation revealed a progressive loss of CD71 expression,
188 consistent with a change in the population structure to one dominated by erythrocytes
189 rather than reticulocytes (Figure 1D).

190

191 To isolate a more homogeneous population of mature cRBCs for invasion assays, we
192 differentiated the cRBCs for 21-22 days and then used anti-CD71 antibody-immobilized
193 magnetic beads to enrich for CD71-negative cells (Figure S4). Using these highly mature
194 cells, invasion assays with *P. falciparum* strain 3D7 showed a ~75% reduction in invasion
195 into the CD55-CRISPR cRBCs as compared to isogenic control cRBCs in three biological
196 replicate experiments (Figure 1E). Since our CRISPR-Cas9 genome editing strategy
197 yielded a mixed population of ~90% CD55-null and 10% CD55-positive cells, we
198 suspected that the residual invasion observed in the "CD55-CRISPR" population was
199 attributable to wild-type cells. This was confirmed by immunofluorescence assays
200 showing that *P. falciparum* invasion was restricted to the cells expressing CD55: the
201 parasitemia in the minority, CD55-positive cells in the population was 22.5%, whereas
202 less than 0.5% of the CD55-null cRBCs were infected (Figure 1F). These results
203 demonstrate that CD55 is critical for *P. falciparum* invasion of fully differentiated cRBCs,
204 mimicking the prior observations with natural CD55-null erythrocytes, and validating
205 CD55 as an essential host factor for *P. falciparum* invasion. Based on previous
206 observations that the expression levels of many RBC surface proteins decline during
207 reticulocyte maturation (Chu et al., 2018; Malleret et al., 2013), we hypothesize that high
208 levels of other receptors important for invasion, such as basigin, may explain the reduced
209 requirement for CD55 for *P. falciparum* invasion of younger, CD71-positive reticulocytes.
210

211 **Antibodies targeting CD55 inhibit *P. falciparum* invasion**

212 To determine if *P. falciparum* invasion can be inhibited using antibodies targeting CD55,
213 we performed in vitro growth assays in the presence of three established anti-CD55
214 monoclonal antibodies individually and in combination. The antibodies each recognize a
215 different short consensus repeat (SCR) in the CD55 ectodomain: BRIC 230, BRIC 110
216 and BRIC 216 target SCR1, SCR2 and SCR3, respectively. While none of the antibodies
217 individually affected parasite growth, we observed a dose-dependent inhibition of parasite
218 growth over 72 hours in the presence of all three anti-CD55 monoclonal antibodies
219 combined, in comparison to an isotype control (Figure 2A). At the highest antibody
220 concentration tested (500µg/ml), the relative parasitemia was reduced by ~40% in the
221 presence of the combined monoclonals, compared to the isotype control.

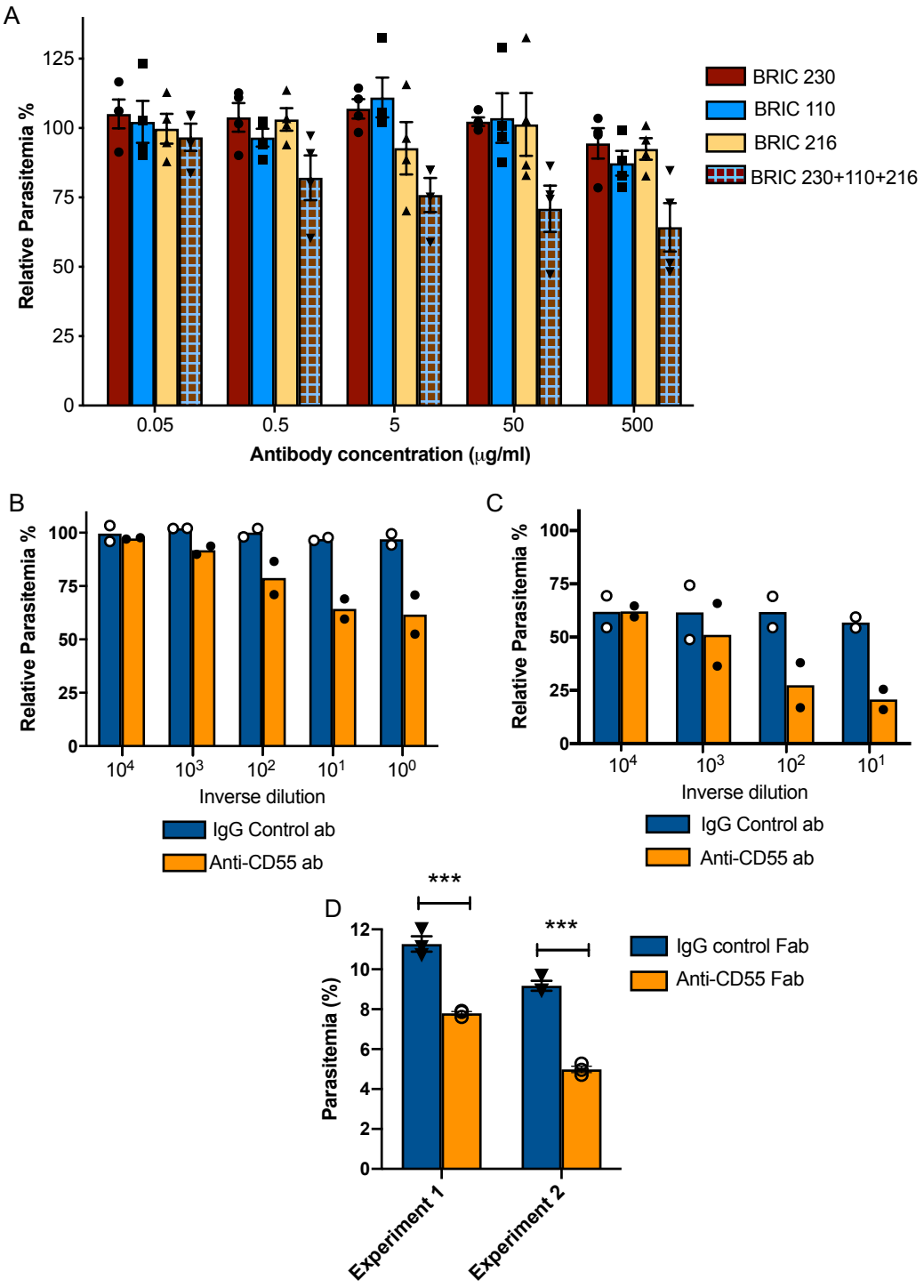

222

223 **Fig 2: Blocking CD55 with antibody inhibits growth of *P. falciparum*** (A) *P. falciparum* strain 3D7
224 parasitemia after 72 hours of growth in RBCS in the presence of increasing concentrations of anti-CD55
225 monoclonal antibodies, relative to isotype control antibody (BRIC 170) at the same concentration. For the
226 pooled antibodies, the indicated concentration was the total combined value, and there were equimolar
227 amounts of each antibody. (N=3 biological replicates; n=2 technical replicates). Error bars indicate SEM.

228 (B) Parasitemia of *P. falciparum* strain 3D7 after 72 hours growth in non-enzyme treated RBCs with
229 increasing concentrations of polyclonal anti-CD55 IgG antibody, relative to that in isotype control antibody
230 at same concentration. (N=2 biological replicates; n=2 technical replicates). The highest antibody
231 concentration (10^0) was 400 ug/ml. (C) As in B, but with neuraminidase-treated RBCs. The highest antibody
232 concentration (10^1) was 40 ug/ml. (D) *P. falciparum* strain 3D7 parasitemia after 72 hours growth in 400
233 ug/ml Fab fragments generated from anti-CD55 polyclonal antibody or isogenic control. Error bars indicate
234 SEM. ***$p<0.005$. The starting parasitemias were 0.3% (Experiment 1) or 0.5% (Experiment 2).
235

236

237 To further study anti-CD55-mediated inhibition of *P. falciparum* invasion, we generated a
238 rabbit polyclonal antibody raised against the entire ectodomain of human erythrocyte
239 CD55. Flow cytometry analysis confirmed that the purified IgG antibody recognizes an
240 antigen on wild-type (WT) RBCs but not on CD55-null RBCs from an Inab donor
241 (Takahashi, 2008), confirming its specificity for CD55 (Figure S5). In *P. falciparum* growth
242 assays, we observed a dose-dependent inhibition of parasite growth in the presence of
243 anti-CD55 antibody relative to isotype control, with a ~40% reduction in relative
244 parasitemia at the highest concentration of antibody (400 μg/ml) (Figure 2B). This degree
245 of inhibition was very similar to that seen for the pooled monoclonal antibodies; together,
246 these findings suggest that blocking CD55 on the RBC can inhibit *P. falciparum* invasion.
247
248 We next tested the effect of anti-CD55 antibody on sialic acid-independent invasion
249 pathways by treating cells with neuraminidase (NM) to remove sialic acid. As has been
250 described previously, the growth of *P. falciparum* strain 3D7 was inhibited ~40% in NM-
251 treated RBCs as compared to untreated cells in the absence of antibody (Figure 2C),
252 reflecting some reliance of strain 3D7 on sialic acid for efficient invasion. In the presence
253 of increasing concentrations of anti-CD55 antibody, we observed a dose-dependent
254 inhibition of parasite growth in the NM-treated cells that is similar to untreated cells (~60%
255 versus ~40% at maximum concentration of antibody) (Figure 2B-C). The finding that
256 CD55 blockade inhibits *P. falciparum* regardless of the presence of membrane sialic acid
257 suggests that CD55 plays a role in both sialic acid-dependent and -independent invasion.
258 These results are consistent with previous findings showing that the requirement for CD55

259 is strain-transcendent, including strains that rely on sialic acid to various degrees (Egan
260 et al., 2015).
261
262 To confirm that the inhibitory effect of the polyclonal anti-CD55 antibody on *P. falciparum*
263 growth was not due to crosslinking, we tested the growth inhibitory activity of monovalent
264 anti-CD55 antibody fragments (Fab fragments). In the presence of 400 µg/ml of anti-CD55
265 Fab fragments, we observed ~40% reduction in relative parasitemia, recapitulating the
266 growth inhibitory activity observed with the bivalent anti-CD55 IgG antibody (Figure 2D).
267 These results further support the conclusion that CD55 is a critical host receptor for *P.*
268 *falciparum*.
269
270 **Blocking CD55 inhibits *P. falciparum* internalization**
271 To specifically determine the impact of CD55 blockade on *P. falciparum* invasion, we used
272 live cell imaging to visualize and quantify schizont rupture and merozoite invasion in real
273 time in the presence of the anti-CD55 polyclonal antibody or an isotype control (Figure
274 3A; Movies S1-S2). First, we quantified the efficiency of merozoite internalization in the
275 presence of anti-CD55 antibody versus isotype control. In the presence of the isotype
276 control antibody, of 345 *P. falciparum* merozoites that contacted an RBC, 53 invaded
277 successfully (15%) (Figure 3B). This frequency is similar to that described in previous live
278 microscopy studies analyzing the efficiency of 3D7 merozoite invasion in the absence of
279 antibodies (Volz et al., 2016; Weiss et al., 2015). In comparison, merozoite invasion was
280 significantly reduced in the presence of anti-CD55 antibody. Out of 312 merozoites that
281 made contact with an RBC in the presence of anti-CD55, only 21 successfully invaded

282 (6.7%) (Figure 3B). The number of invasion events per schizont rupture was similarly
283 reduced by half in the presence of anti-CD55 compared to control antibody (Figure 3C),
284 indicating that anti-CD55 antibody inhibits entry but does not prevent initial contact
285 between the merozoite and RBC.
286
287 **Blocking CD55 has no impact on pre-invasion kinetics**
288 Next, we examined the impact of CD55 blockade on the kinetics of the three main phases
289 of *P. falciparum* invasion: the pre-invasion time (period from initial contact to the onset of
290 internalization), the internalization time, and the time to echinocytosis (transient period of
291 cell dehydration that occurs after internalization) (Dvorak, Miller, Whitehouse, & Shiroishi,
292 1975; Weiss et al., 2015). For the subset of merozoites that ultimately invaded
293 successfully, there was no difference in the length of the pre-invasion time, internalization
294 time, or time to echinocytosis in the presence of anti-CD55 antibody compared isotype
295 control (Figure 3D-F). These results indicate that blocking CD55 does not impact pre-
296 invasion kinetics, at least not for the merozoites that manage to invade in the presence
297 of antibody.
298

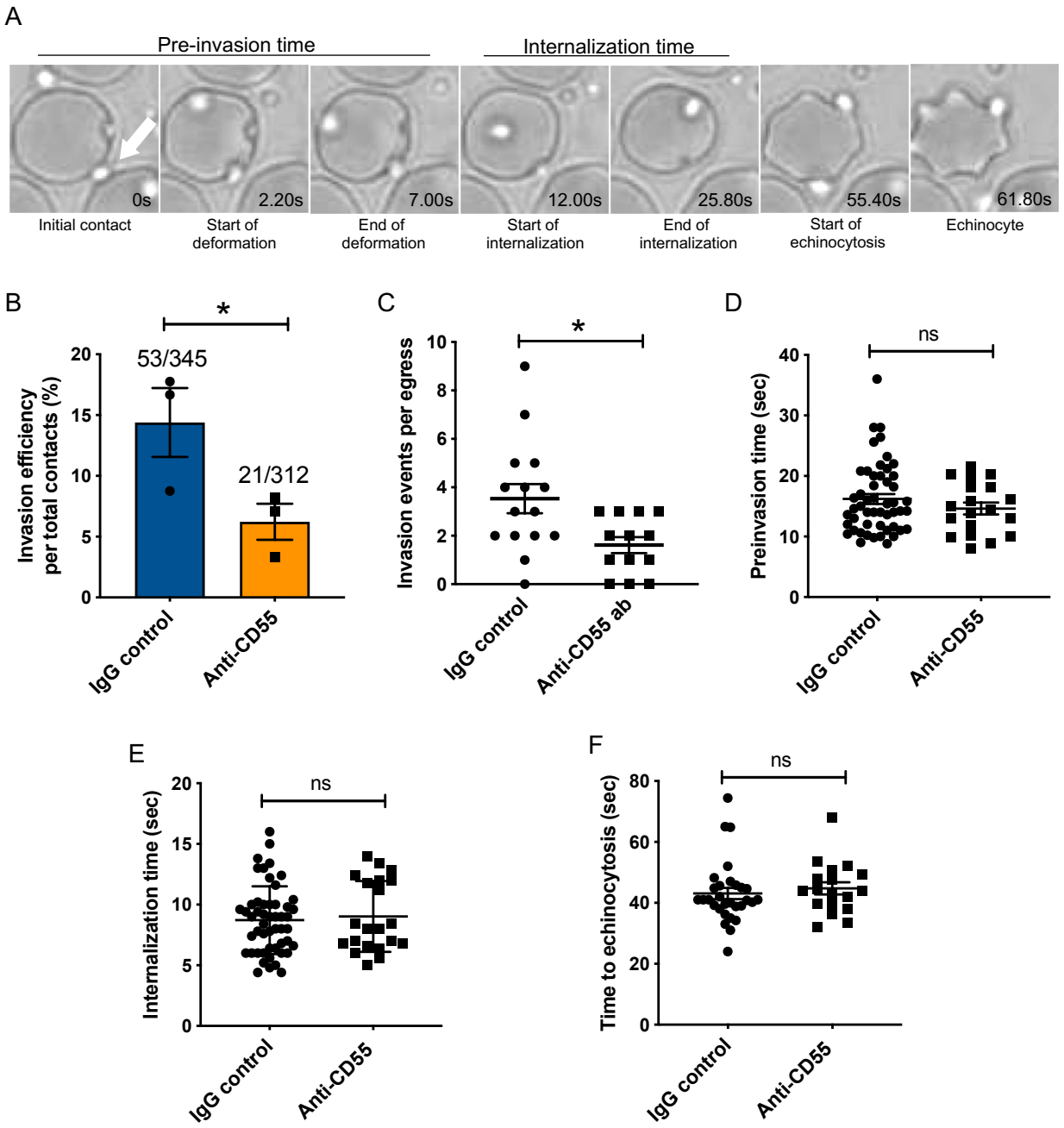

Fig 3: Blocking CD55 with antibody inhibits invasion but not pre-invasion kinetics (A) Time-lapse images of invasion after initial merozoite contact. Arrowhead indicates invading merozoite. Time in seconds. (B) Percentage of merozoites that invaded an RBC after initial contact in presence of polyclonal anti-CD55 antibody (anti-CD55) or isotype control (IgG control). Bottom number is the total number of merozoites followed that made contact with the RBC, and top number is the subset that invaded. The data were acquired in three independent experiments, and the dots indicate the mean invasion efficiency from each experiment; *p=0.03. (C) Number of successful invasion events per schizont rupture (egress) in presence of anti-CD55 antibody or isotype control; *p=0.01. (D) Pre-invasion time (in seconds) for merozoites that

308 contact an RBC in the presence of anti-CD55 antibody or isotype control. (E) Internalization time (in
309 seconds) for merozoites in the presence of anti-CD55 antibody or isotype control antibody. (F) Time to
310 echinocytosis from the end of merozoite internalization in the presence of anti-CD55 antibody or isotype
311 control. Error bars indicate SEM; ns, not significant (B-F).
312

313 **Merozoite-induced erythrocyte deformation is unaffected by CD55 blockade**

314 During the pre-invasion period, parasite attachment to the RBC is associated with
315 substantial deformation of the host cell membrane as the merozoite reorients apically
316 (Dvorak et al., 1975; Gilson & Crabb, 2009; Paul et al., 2015). The degree of deformation
317 is variable, and is mediated by interactions between parasite ligands released from the
318 apical microneme organelles, such as the EBAs and Rhs, and receptors on the RBC
319 membrane (Weiss et al., 2015). To investigate whether CD55 plays a role in RBC
320 deformation, we used live microscopy to quantitate the efficiency and kinetics of
321 merozoite-induced RBC deformation in the presence of anti-CD55 antibody versus
322 isotype control. The efficiency of deformation was similar in the presence of the two
323 antibodies: approximately 67% of merozoites deformed the RBC in the presence of anti-
324 CD55 antibody, compared to ~60% deformation efficiency with the isotype control (Figure
325 4A). In addition, there was no significant difference in the duration of the deformation
326 period in the presence of the two different antibodies (Figure 4B), suggesting that CD55
327 does not influence merozoite-induced deformation.

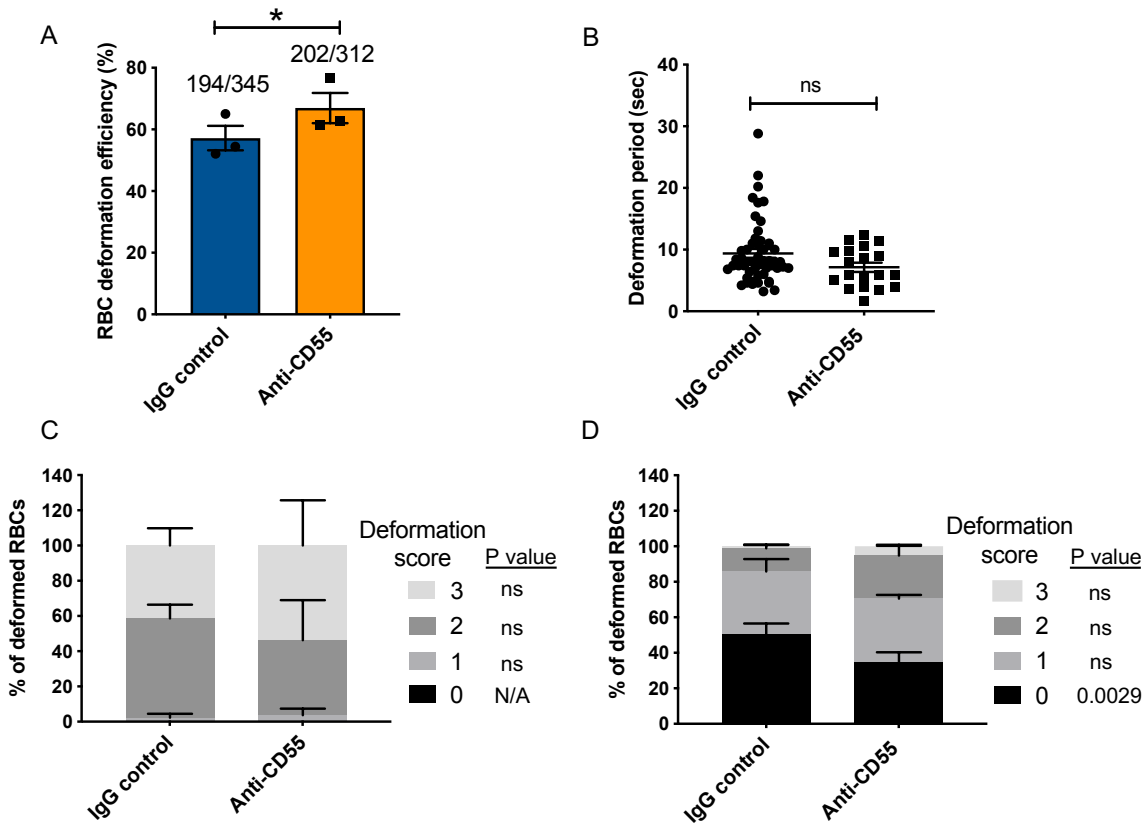

Fig 4: Merozoite-induced erythrocyte deformation is not affected by blocking CD55 (A) Efficiency of RBC deformation by merozoites that make contact in presence of anti-CD55 or IgG control. The fractions indicate the number of deformed RBCs out of the total merozoite-RBC contacts observed. The data were acquired in three independent experiments, and the dots represent the mean for each experiment.; *p=0.02. **(**B) Duration of erythrocyte deformation induced by attached merozoites that ultimately invaded in presence of polyclonal anti-CD55 antibody (anti-CD55) or isotype control (IgG control). Time in seconds. (C-D) Strength of merozoite-induced deformation in presence of anti-CD55 or isotype control for cases where invasion was successful (C) or not successful (D); N/A, not applicable; ns, not significant, *p=0.0029. Error bars indicate SEM (A-D).

339 We employed a four-point deformation scale to quantify the intensity of merozoite-induced
340 RBC deformation in the presence of antibody, where 0 denotes the absence of
341 deformation and 3 denotes the most extreme degree of deformation (Weiss et al., 2015)
342 (Movies S3-S5). Almost all merozoites that invaded successfully induced strong
343 deformation (scores of 2 or 3), regardless of which antibody was present (Figure 4C). In
344 comparison, merozoites that failed to invade had lower deformation scores, the majority
345 having scores of 0 or 1. For these merozoites, the distribution of scores skewed higher
346 in the presence of anti-CD55 antibody compared to the isotype control, perhaps reflecting
347 the inability of otherwise "fit" merozoites to complete invasion (Figure 4D). Taken
348 together, these findings demonstrate that blocking CD55 with antibody does not influence
349 the efficiency, duration, or strength of merozoite-induced RBC deformation, and instead
350 suggest that CD55 exerts its effect on invasion at a downstream step.
351
352 To further validate the conclusions of the antibody inhibition experiments, we took a
353 complementary approach and performed live cell imaging of *P. falciparum* invasion with
354 natural CD55-null erythrocytes from a rare donor with the Inab phenotype, where CD55
355 is absent due to a stop codon in exon 2(Takahashi, 2008). In traditional invasion assays,
356 we observed ~80% reduction in the efficiency of *P. falciparum* invasion into CD55-null
357 RBCs as compared to control RBCs after ~ 18 hours, as has been shown previously
358 (Egan et al., 2015) (Figure S6). When imaging invasion in real time, we did not observe
359 any successful invasion events into the CD55-null RBCs, out of 310 merozoites that made
360 contact (Figure 5A and Movies S6-S7). In comparison, there were 25 successful invasion
361 events into the control RBCs, out of 197 merozoites that made contact (~11%). Although

362 invasion into the CD55-null cells was clearly impaired, there was no difference in the
363 efficiency of merozoite-induced RBC deformation between the two genetic backgrounds
364 (Figure 5B). Moreover, we observed no significant difference in the distribution of
365 deformation scores between CD55 null and control RBCs for merozoites that did not
366 invade (Figure 5C). These results are consistent with the findings from the antibody
367 inhibition experiments, and suggest that CD55 influences invasion by acting after the
368 period of erythrocyte deformation.

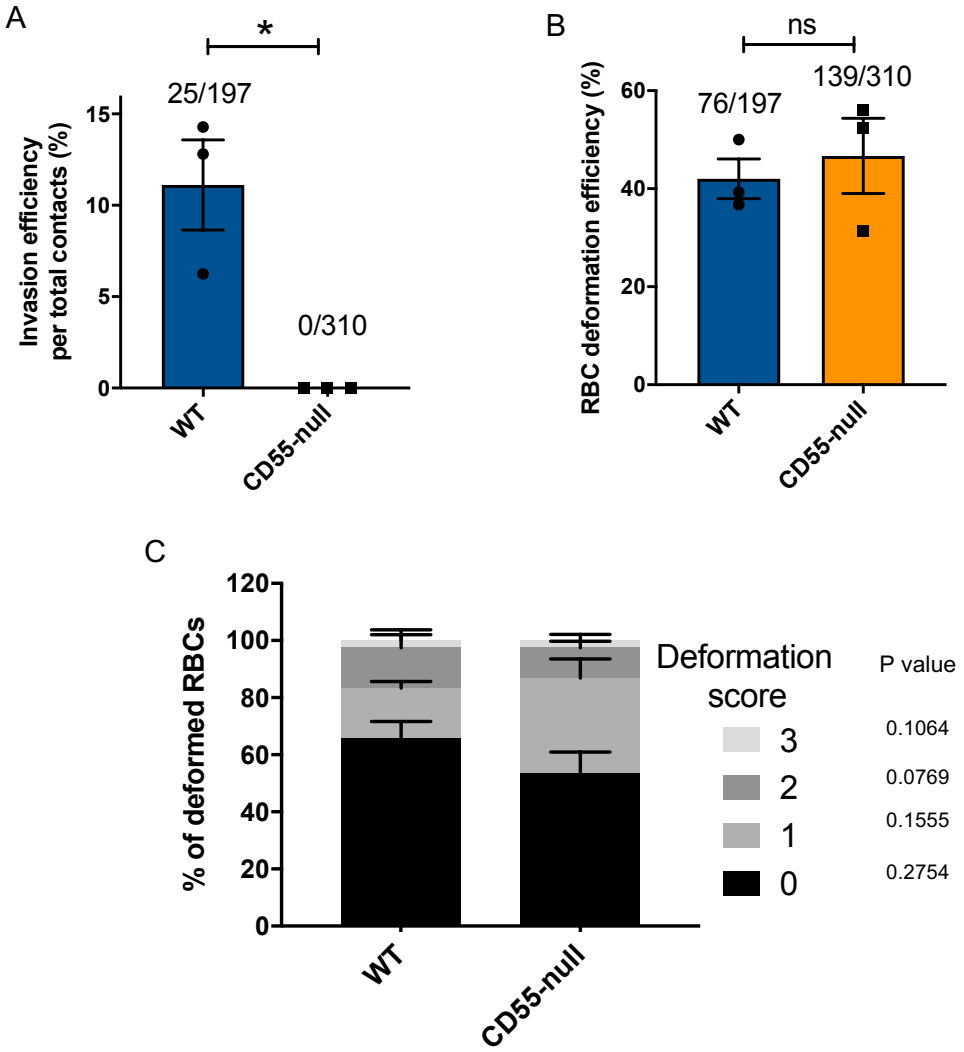

369

370 **Fig 5: Absence of CD55 prevents invasion but does not impact deformation. (**A) Percentage of
371 merozoites that invaded wild-type (WT) or CD55-null RBCs after initial contact. Bottom number is the total

372 number of merozoites followed that made contact with the RBC, and top number is the subset that invaded.
373 The data were acquired in three independent experiments, and the dots indicate the mean invasion
374 efficiency from each experiment; *p=0.04. (B) Efficiency of WT or CD55-null RBC deformation upon
375 merozoite contact. Bottom number is the total number of RBCs contacted by a merozoite, and top number
376 is the subset that were deformed upon contact. The data were acquired in three independent experiments,
377 and the dots indicate the mean deformation efficiency for each experiment; ns, not significant. (C) Strength
378 of merozoite-induced deformation of WT or CD55-null RBCs among non-invading merozoites; ns, not
379 significant. Error bars indicate SEM (A-C).
380

381

382 **CD55 acts downstream of rhoptry discharge**

383 Since we observed that the blocking or deletion of CD55 impaired *P. falciparum* entry
384 without altering pre-invasion kinetics or membrane deformation, we hypothesized that
385 CD55 functions after the ligand-receptor interactions that mediate attachment and
386 deformation. During the sequential steps of *P. falciparum* invasion, RBC deformation is
387 followed by injection of the rhoptry organelle contents into the host cell cytoplasm, an
388 event that requires an interaction between the parasite ligand PfRh5 and its RBC
389 receptor, basigin (Weiss et al., 2015). The contents of the rhoptries in turn are believed
390 to trigger echinocytosis. When the interaction between PfRH5 and basigin is blocked
391 using inhibitory antibodies and rhoptry discharge is prevented, echinocytosis fails to occur
392 (Volz et al., 2016; Weiss et al., 2015). To investigate whether CD55 is similarly required
393 for release of the rhoptry contents, we quantified the incidence of RBC echinocytosis
394 elicited by attached merozoites in the presence of anti-CD55 antibody versus isotype
395 control using a cytochalasin-D (cyt-D) live microscopy assay (Figure 6A-B and Movie S8).
396 Cyt-D is an inhibitor of actin polymerization that prevents merozoite internalization by
397 inhibiting the actino-myosin motor, but does not impact attachment, rhoptry discharge, or
398 echinocytosis (Miller, Aikawa, Johnson, & Shiroishi, 1979; Weiss et al., 2015). Upon
399 treatment with cyt-D, ~60% of merozoites that attached to an RBC triggered echinocytosis
400 in the presence of the isotype control antibody, and a similar rate of echinocytosis was
401 observed in the presence of anti-CD55 antibody (Figure 6C). These results demonstrate
402 that blocking CD55 does not significantly impact rhoptry discharge or echinocytosis,
403 standing in distinct contrast to what has been observed for basigin and Rh5, where
404 blocking their interaction with antibodies prevents echinocytosis (Weiss et al., 2015).

405 Together, these findings demonstrate that CD55 acts downstream of the interaction
406 between RH5 and basigin, facilitating a step of invasion that occurs after release of the
407 rhoptry organelles.

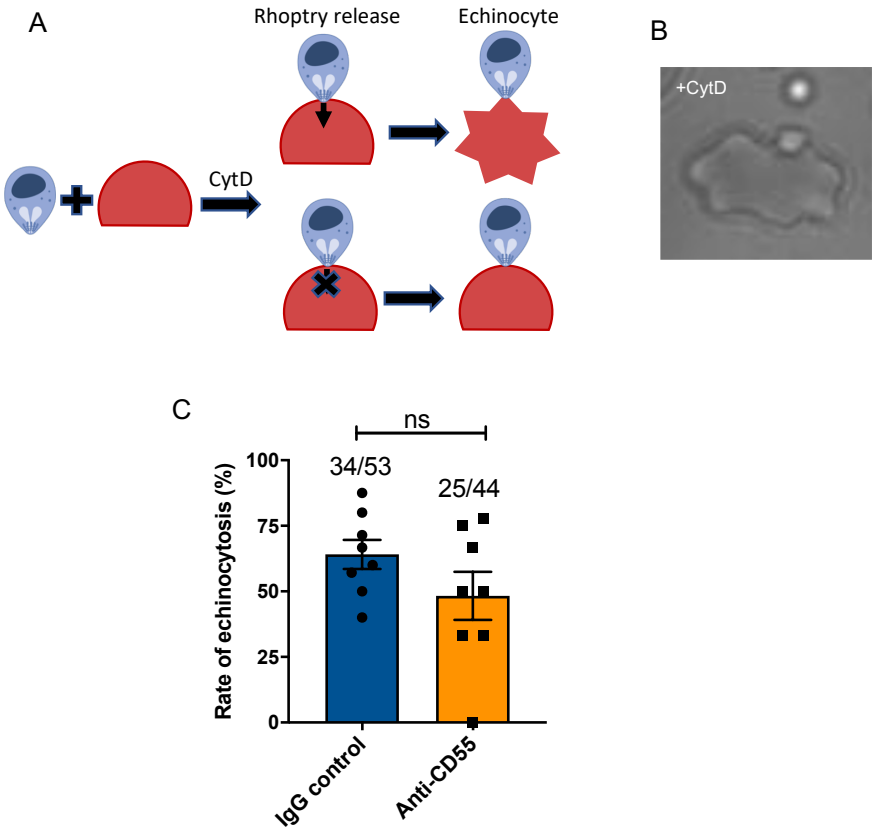

Fig 6: Blocking CD55 with antibody does not impact echinocytosis. (A) Cartoon illustrating echinocytosis elicited by an attached merozoite that has discharged its rhoptry contents in the presence of cyt-D, which prevents internalization. Reagents that block rhoptry discharge prevent echinocytosis. (B) Image showing an echinocyte with an attached merozoite. Scale bar=5um. (C) Echinocytosis efficiency in the presence of anti-CD55 antibody or isotype control. Bottom number is the total number of merozoite-RBC pairs observed to make contact, and top number is the subset in which echinocytosis occurred. The data are from eight independent experiments. Dots indicate the mean from each experiment and error bars represent the standard error of mean; ns, not significant.

408

409

410 **CD55 may be required for progression of the moving junction**

411 The moving junction that forms between the cell membranes of an invading merozoite
412 and the erythrocyte during internalization involves interactions between PfAMA1, which
413 derives from the micronemes, and the PfRON complex, which is expressed by the
414 rhoptries. To investigate a possible role for CD55 in formation of the moving junction, we
415 sought to visualize PfAMA1 and PfRON4 as merozoites attempted to invade CD55-null
416 (Inab) or wild-type erythrocytes in the presence of cyt-D. Under these conditions, we
417 observed a ~50% reduction in the efficiency of merozoite attachment to CD55-null
418 erythrocytes as compared to WT controls by flow cytometry, as has been observed
419 previously (Figure 7A) (Egan et al., 2015). Using confocal microscopy, we found that
420 PfAMA1 and PfRON4 were frequently co-localized at the cellular interface for merozoites
421 attached to WT control cells (~85%) (Figure 7B). In comparison, for merozoites attached
422 to CD55-null erythrocytes, PfAMA1 and PfRON4 were co-localized at the cellular
423 interface in only ~40% of cases (Figure 7B). For those merozoites in which PfAMA1 and
424 PfRON4 were colocalized at the interface, we observed that approximately half of the WT
425 control cells had an indentation at the point of merozoite contact, suggesting the
426 merozoites were mid-invasion, whereas this was never observed for the CD55-null cells
427 (Figure 7C). Together, these results support a model where CD55 is required for
428 progression of the moving junction, and acts downstream of and distinctly from all other
429 known host receptors for *P. falciparum* invasion.

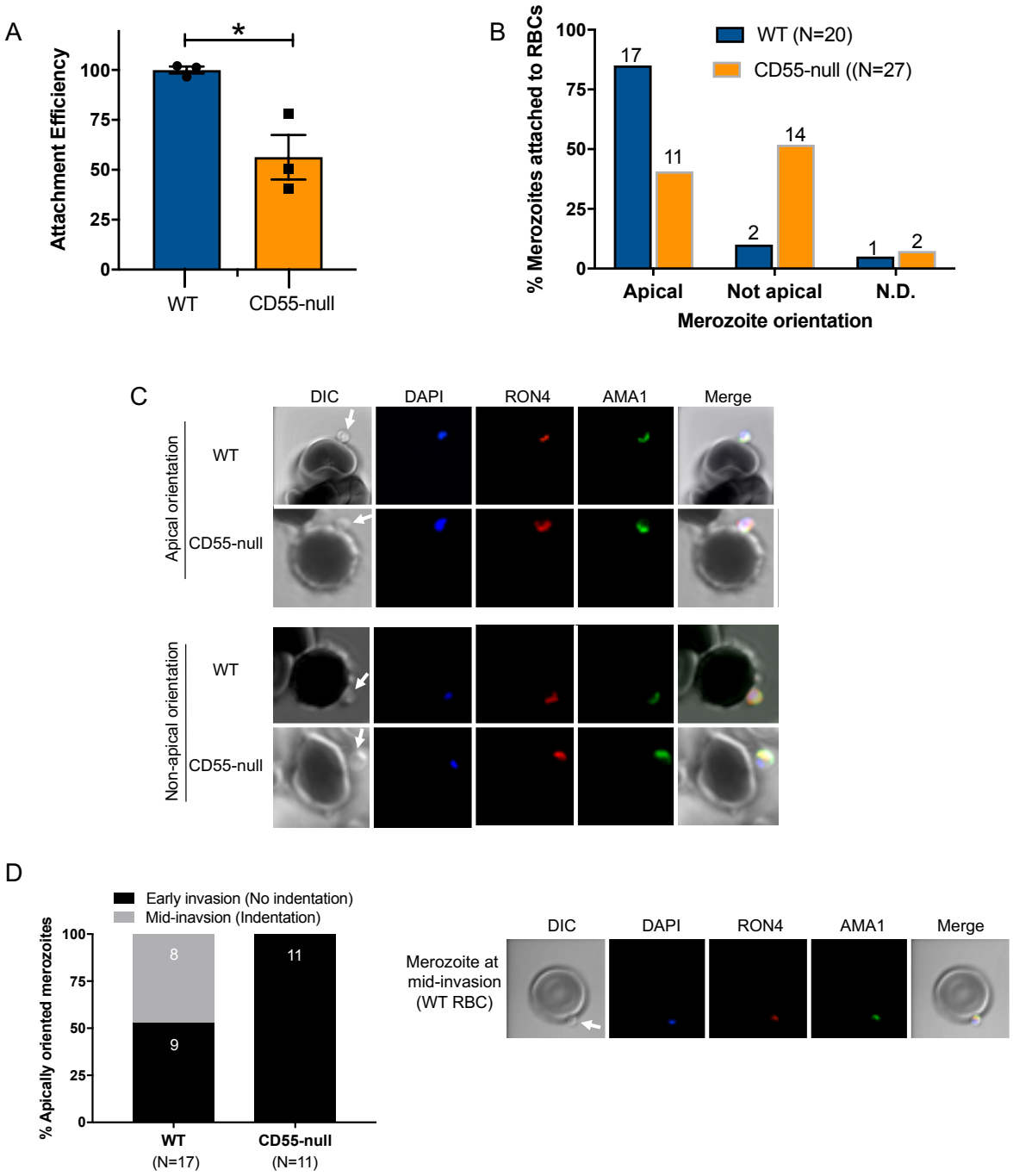

Fig 7: Invasion fails to progress in the absence of CD55.

(A) Attachment efficiency of *P. falciparum* merozoites to CD55-null versus control RBCs in the presence of cyt-D, as measured by flow cytometry 90 min after the addition of synchronized schizonts (N=3, n=3). Error bars indicate SEM; *p<0.018. (B) Orientation of merozoites attached to WT versus CD55-null RBCs, indicated by the localization of AMA1, RON4, and a density at the merozoite's apical end as measured by confocal microscopy. Apical, AMA1 and RON4 co-localized at the cellular interface and merozoite density abutting RBC; Not apical, AMA1 and RON4 not co-localized at the cellular interface and merozoite density

438 not abutting RBC; N.D., indeterminate. The numbers above each bar indicate the subset of attached
439 merozoites in that orientation. (C) Representative confocal images showing merozoites attached to RBCs
440 with apical or non-apical orientation. Merozoite density at the apical end of the merozoite is indicated by an
441 arrow. (D) Progression of invasion for merozoites apically attached to CD55-null or WT RBCs in the
442 presence of cyt-D. Panel on the right shows representative confocal images of a merozoite at the mid-
443 invasion stage.
444

445 **Discussion**

446 A comprehensive understanding of the molecular interactions required for *P. falciparum*
447 invasion has been limited by the absence of a robust genetic system to study red cells,
448 which are terminally differentiated and lack a nucleus and DNA. Previously, an RNAi-
449 based forward genetic screen in cultured red cells derived from HSPCs identified two new
450 candidate host factors for invasion: CD44 and CD55 (Egan et al., 2015). In this study, we
451 used a combination of genetics and inhibitory antibodies to determine the precise steps
452 of *P. falciparum* invasion during which CD55 functions. We have demonstrated that CD55
453 is specifically required for merozoite internalization, and plays a unique role relative to the
454 other host receptors known to act during invasion.

455 Prior work has shown that the efficiency of *P. falciparum* infection is reduced by ~
456 50% in CD55-deficient cRBCs where expression is downregulated using shRNAs. While
457 experiments using erythrocytes from two rare, CD55-null donors suggested that CD55 is
458 essential for *P. falciparum* invasion, this has never been demonstrated genetically. A
459 major roadblock to such experiments has been the technical challenges associated with
460 CRISPR-Cas9 genome editing in primary human hematopoietic stem cells, including
461 cytotoxicity from nucleic acids and low rates of transfection (Hendel et al., 2015). In this
462 study, we showed for the first time that fully mature, CD55-null cRBCs can be generated
463 efficiently from primary human HSPCs using CRISPR-Cas9 genome editing. Using
464 isogenic wild-type and mutant cells, we have demonstrated that CD55-null cRBCs are
465 resistant to *P. falciparum* invasion, confirming that CD55 is an essential host factor for *P.*
466 *falciparum*.

467

468 Here, we demonstrated the feasibility and benefits of generating truly mature erythrocytes
469 ex-vivo for the study of malaria host factors, as these cells closely mimic the target cell
470 for *P. falciparum* in the human bloodstream. Our approach involving the co-delivery of
471 two chemically modified sgRNAs together with Cas9 as a ribonucleoprotein complex has
472 been shown to be an effective strategy for CRISPR-based gene knockout in primary
473 HSPCs and T cells (Hendel et al., 2015). This method obviates the toxicity associated
474 with plasmid delivery, minimizes off-target activity, and improves sgRNA stability.
475 Combined with our ex-vivo erythropoiesis culture system, this method can efficiently
476 generate terminally differentiated, enucleated, CD71-low red cells with a high rate of gene
477 knock out that can be used to study host genetic determinants for *P. falciparum* in an
478 isogenic background.
479
480 We observed that the reliance of *P. falciparum* on CD55 for invasion increased
481 significantly as enucleated cRBCs matured into erythrocytes, likely reflecting the
482 substantial changes in protein abundance that occur during terminal maturation of human
483 red cells, including for proteins known to act as receptors, such as basigin and CR1
484 (Gautier et al., 2016; G. Hu et al.). The efficiency of *P. falciparum* invasion is further
485 influenced by the deformability of the red cell membrane (Tiffert et al., 2005), a biophysical
486 property that also changes as red cell progenitors proceed through enucleation and final
487 maturation (Giarratana et al., 2005). As clinical malaria is primarily a disease of mature,
488 peripheral blood erythrocytes, our results showing that terminal red cell maturation
489 modifies the requirement for CD55 during invasion highlights the potential drawbacks of
490 using cell lines to study host factors for *P. falciparum*. While considered erythroid in

491 nature, immortalized cell lines such as JK-1, EJ and BEL-A have low rates of enucleation
492 and terminal maturation (Kanjee et al., 2017; Satchwell et al., 2019; Scully et al., 2019),
493 suggesting their utility for genetic experiments on *P. falciparum* invasion may be limited
494 by incomplete phenotypes.
495
496 Antibodies targeting a variety of specific host receptors for *P. falciparum* have been
497 shown to have invasion inhibitory activity, including those against GYPA, CR1, and
498 basigin (Crosnier et al., 2012; Pasvol et al., 1989; Spadafora et al., 2010). While we found
499 that individual monoclonal antibodies against three distinct SCR domains of CD55 had
500 no discernable effect on *P. falciparum* growth, in combination they had potent dose-
501 dependent inhibitory activity, suggesting CD55's role in invasion is not restricted to a
502 specific SCR domain. Our demonstration that both the polyclonal anti-CD55 antibody and
503 anti-CD55 Fab fragments can inhibit *P. falciparum* growth aligns with the results from our
504 genetic studies, and corroborates the conclusion that CD55 is a critical host factor for *P.*
505 *falciparum*. In contrast to CR1, where antibodies are only inhibitory in the absence of red
506 cell sialic acid (Spadafora et al., 2010), anti-CD55 antibody blocked both sialic acid-
507 dependent and -independent invasion. This finding is consistent with prior studies
508 showing that the requirement for CD55 in *P. falciparum* invasion is strain-transcendent
509 (Egan et al., 2015), and implies a model where CD55 acts distinctly from CR1 and the
510 other alternative, strain-specific receptors.
511
512 Given the inherent limitations associated with studying invasion on a population scale in
513 longer term assays, live microscopy has been increasingly employed to visualize

514 individual *P. falciparum* invasion events in real time. Analysis of the morphology and
515 kinetics of discrete invasion steps in the context of blocking antibodies or soluble proteins
516 has contributed to a model describing the molecular events that occur during invasion
517 (Volz et al., 2016; Weiss et al., 2015). Our live microscopy experiments have added a
518 new dimension to this model by revealing that merozoite internalization is inhibited in the
519 presence of anti-CD55 antibody or with CD55-null erythrocytes, demonstrating for the first
520 time that CD55 is specifically required for parasite entry. Where and how does CD55 act
521 in relation to the *P. falciparum* ligands and erythrocyte receptors known to function during
522 invasion? We observed no impact of the anti-CD55 antibody on pre-invasion kinetics or
523 merozoite-induced erythrocyte deformability, findings that were validated using CD55-null
524 erythrocytes from a rare donor. These results suggest that CD55 functions distinctly from
525 the "alternative" receptors required for apical reorientation and red cell deformation (e.g.
526 glycophorins and CR1), as blocking interactions between these receptors and their
527 ligands strongly inhibits merozoite-induced deformability (Weiss et al., 2015).
528
529 Echinocytosis is a phenomenon of transient red cell shrinkage that commences soon after
530 merozoite internalization. Current evidence suggests that it is stimulated by changes in
531 the red cell cytoplasm that occur once an irreversibly-attached merozoite discharges its
532 rhoptry contents into the erythrocyte (Volz et al., 2016; Weiss et al., 2015). Echinocytosis
533 is inhibited by antibodies that block the interaction between PfRH5 and basigin, implying
534 that this interaction is necessary for rhoptry discharge (Weiss et al., 2015). These blocking
535 antibodies also inhibit Ca^{2+} flux into the erythrocyte, possibly reflecting formation of a pore
536 at the cellular interface when PfRH5 and basigin interact (Volz et al., 2016). The

537 glycophorins and CR1 act early in the pre-invasion phase during apical reorientation, and
538 blocking their interactions with ligands using genetics, enzyme treatments, or antibody
539 blockade also inhibits echinocytosis (Volz et al., 2016; Weiss et al., 2015). In contrast,
540 echinocytosis is not prevented by treatment with the actin polymerization inhibitor cyt-D
541 or reagents that block the interaction of PfAMA1 and the RON complex. Together, these
542 findings demonstrate that the stimulus for echinocytosis occurs after the interaction of
543 PfRH5 with basigin, but before establishment of the moving junction.
544
545 Our observation that anti-CD55 antibody had no effect the efficiency of merozoite-induced
546 echinocytosis demonstrates that CD55 acts distinctly from basigin and the other
547 established host receptors known to act during *P. falciparum* invasion. While both anti-
548 CD55 and anti-basigin inhibit invasion, echinocytosis occurs normally in the presence of
549 anti-CD55 but is blocked by anti-basigin antibody, likely due to inhibition of rhoptry
550 discharge (Volz et al., 2016). As blocking CD55 does not inhibit deformation nor
551 echinocytosis during invasion, our findings support a model in which CD55 acts after
552 rhoptry discharge, and specifically impacts merozoite internalization.
553
554 Merozoite internalization requires the formation of a moving junction between the cell
555 membranes of the invading merozoite and the erythrocyte that moves posteriorly down
556 the parasite as it invades. The current model of the moving junction involves interactions
557 between PfAMA1 expressed on the merozoite surface and the PfRON complex inserted
558 into the red cell membrane, independent of any host-encoded receptors (Alexander et al.,
559 2006; Alexander et al., 2005; Besteiro et al., 2009; Richard et al., 2010; Riglar et al., 2011;

560 Srinivasan et al., 2011). In addition to its key role in internalization, the moving junction
561 has also been proposed to be important for formation of the parasitophorous vacuole (PV)
562 (Yap et al., 2014).
563
564 Could CD55 function as a component of the moving junction during invasion? We
565 observed that PfAMA1 and PfRON4 were almost always co-localized at the cellular
566 interface for merozoites attempting to invade WT cells, whereas this was significantly less
567 common for merozoites attempting to invade CD55-null erythrocytes. For the minority of
568 merozoites that attached to CD55-null erythrocytes and had PfAMA1 co-localized with
569 RON at the cellular interface, none were observed to have progressed past early invasion,
570 unlike those attached to WT cells. Together, these findings support a model in which
571 CD55 is required for progression of the moving junction, either directly or indirectly. Future
572 studies involving higher resolution microscopy such as cryo-EM will be necessary to
573 better characterize how absence of CD55 may impact the moving junction or architecture
574 of the PV after invasion.
575
576 Our findings showing that the function of CD55 during invasion can be narrowed to the
577 internalization step are consistent with a model where CD55 acts distinctly from the other
578 known receptors for invasion, potentially by interacting with a specific parasite ligand. As
579 there is a precedent for CD55 on epithelial cells to act as a pathogen receptor that
580 transmits signals to the host cell (Coyne & Bergelson, 2006), it is tantalizing to
581 hypothesize that this molecule functions similarly in *P. falciparum* invasion of
582 erythrocytes. Ultimately, biochemical identification of parasite and erythrocyte interaction

583 partners of CD55 will yield important additional insights into the molecular function of
584 CD55 during merozoite internalization. Given the complexity of *P. falciparum* invasion and
585 the unique and essential role of CD55 relative to other established receptors, targeting its
586 activity or interaction partners in novel intervention strategies may enhance the
587 effectiveness of future therapies or vaccines for malaria.
588

589 **Methods**

590 ***P. falciparum* culture, invasion assays and growth inhibition assays**

591 *P. falciparum* strain 3D7, a laboratory-adapted strain obtained from the Walter and Eliza
592 Hall Institute (Melbourne, Australia) was routinely grown in human erythrocytes (Stanford
593 Blood Center) at 2% hematocrit in complete RPMI-1640 supplemented with 25 mM
594 HEPES, 50 mg/L hypoxanthine, 2.42 mM sodium bicarbonate and 0.5% Albumax
595 (Invitrogen) at 37°C in 5% CO_2 and 1% O_2.
596

597 Parasite invasion assays were performed using synchronized late-stage schizont
598 parasites isolated using a MACS magnet (Miltenyi) and added at 1.0-1.5% initial
599 parasitemia to the cultured red blood cells (cRBCs) or peripheral red blood cells (pRBCs)
600 at 0.3% hematocrit. For some invasion assays, cRBCs were enriched for the CD71
601 negative population by using anti-CD71 antibody immobilized magnetic beads (Miltenyi),
602 as described below. Assays were performed in a volume of 100 μl per well in a 96 well
603 plate, or at 50 μl per well in Half Area 96-well plates (Corning) for the assays with CD71-
604 negative cRBCs. The ring stage parasitemia was determined after 18-24 hours by bright-
605 field microscopy of cytospin preparations stained with May-Grünwald and Giemsa. A

606 minimum of 1000 cells were counted for each technical replicate. For assays in which
607 there was no selection for CD71-negative cells, the invasion efficiency was determined
608 by normalizing the average ring stage parasitema in each genetic background to the
609 average ring stage parasitemia in control peripheral blood RBCs (pRBCs) for each
610 biological replicate. For assays that used CD71-negative cRBCs, the ring stage
611 parasitema for each genetic background was normalized to the mean for the control
612 cRBCs. Assays were performed at least 3 times using 2-3 technical replicates.
613
614 Antibody inhibition assays were performed using pRBCs in the presence of mouse
615 monoclonal antibodies obtained from IBGRL (BRIC 216, BRIC 230, BRIC 110, BRIC
616 170), polyclonal anti-CD55 antibody produced by New England Peptide, or isotype control
617 rabbit IgG antibody (Novus). All antibodies were dialyzed overnight in RPMI buffer prior
618 to use. Schizont stage parasites were added to untreated or neuraminidase treated
619 pRBCs at 0.5% hematocrit at an initial parasitemia of 0.5% in the presence of 0.05 to 500
620 μg/ml of the antibodies. For the neuraminidase treatment, the cells were incubated with
621 66.7mU/ml of neuraminidase from *Vibrio cholerae* (Sigma) at 37°C for 1 h with shaking
622 and washed 3 times in buffer before use in the growth inhibition assays. Some assays
623 were performed in presence of Fab fragments of anti-CD55 or isotype control IgG
624 antibodies at the concentration of 400 μg/ml. The Fab fragments were prepared as
625 described below. Assays were performed 2-3 times with 2-3 technical replicates in a
626 volume of 100 μl per well in 96 well plates. Parasitemias were determined on day 3 by
627 staining with SYBR Green 1 nucleic acid stain (Invitrogen) at 1:2000 dilution in PBS/0.3%

628 BSA for 20 minutes, followed by flow cytometry analysis on a MACSQuant flow cytometer
629 (Miltenyi).
630
631 **Generation of Fab fragments**
632 Polyclonal anti-CD55 antibody and control IgG were digested using the Pierce™ Fab
633 preparation kit (Thermo Fisher Scientific). The resulting Fab fragments were quantified
634 on a spectrophotometer, concentrated, and buffer exchanged with incomplete RPMI
635 using 30K Amicon Ultra 0.5 ml centrifugal filter (Millipore). For final quantification, the Fab
636 fragments were stained with Coomassie in a 10% SDS-PAGE gel along with known
637 concentrations of the undigested antibodies, and concentrations of the Fab fragments
638 were determined using ImageJ 1.50i(Schneider, Rasband, & Eliceiri, 2012).
639
640 **Generation of cultured red blood cells from primary human CD34+ HSPCs**
641 Bone marrow-derived primary human CD34+ HSPCs (Stem Cell Technologies) were
642 cultured in erythroid differentiation medium (cPIMDM) composed of Iscove Basal Medium
643 (IMDM) (Biochrom) supplemented with 4mM L-Glutamine (Sigma), 330 µg/ml holo-
644 transferrin (BBI Solutions), 10 µg/ml of recombinant human insulin (Sigma), 2 IU/ml
645 heparin (Affymetrix), 10^{-6} M hydrocortisone (Sigma), 100ng/ml SCF (R & D Systems), 5
646 ng/ml IL-3 (R & D Systems), 3 IU/ml Epo (Amgen) and 5% plasma (Octapharma) at 37°C
647 in 5% CO2 in air, as previously described (Egan et al., 2015; Giarratana et al., 2011). On
648 the 2nd day of the culture, the cells were subjected to nucleofection with ribonucleoprotein
649 (RNP) complexes as described below. On day 5, the cells were washed and resuspended
650 in fresh cPIMDM to maintain concentration ~ $1x10^4$/ml. Between day 8-13, the cells were

651 maintained in fresh cPIMDM devoid of IL3 and hydrocortisone at concentration of <$5x10^5$
652 cells/ml. On day 13, the cells were washed and plated at $7.5x10^5$ - $1.0x10^6$cells/ml in
653 cPIMDM without IL-3, hydrocortisone, or SCF. On day 15-16, the cells were co-cultured
654 at $1.0x10^6$cells/ml concentration on a murine stromal cell layer (MS-5), as previously
655 described (Giarratana et al., 2005). The cells were harvested on days 18-22 for different
656 experiments. Growth and differentiation were monitored using hemocytometer-based
657 quantification and light microscopy of cytospin preparations stained with May-Grünwald
658 and Giemsa. To quantify the enucleation rate, cRBCs were incubated in Vybrant
659 DyeCycle violet (Life Technologies) (1:10,000) at 37°C for 30 min, followed by flow
660 cytometry analysis on a MACSQuant flow cytometer (Miltenyi).
661

662 **CRISPR-Cas9 genetic modification of primary human CD34+ cells**

663 Two sgRNAs targeting human *CD55* exons were designed using the Broad Institute's
664 GPP sgRNA design portal and synthesized as chemically modified sgRNAs by Synthego.
665 The sgRNA sequences were: GGGCCCCUACUCACCCCACA, which is predicted to
666 recognize a sequence in exon 1 of *CD55*, and CUGGGCAUUAGGUACAUCUG, which is
667 predicted to recognize a sequence in exon 2. Ribonucleoprotein (RNP) complexes
668 containing one or both sgRNAs were prepared by slowly adding 300 pmol of each sgRNA
669 to 150 pmol Cas9 protein in a 10 µl final volume with nuclease-free water and incubating
670 at room temperature for 10 min. On day 2 after thawing CD34+ cells, the RNP complexes
671 were added to $1X10^5$ cells in 40 µl of P3 nucleofection buffer from the 4D-Nucleofector X
672 kit (Lonza). Half of the mixture was loaded to each well of a 16-well nucleofection cassette
673 and nucleofected using the using E0-100 program with the 4D-Nucleofector Lonza

674 Amaxa. After nucleofection, cells were transferred to 6 ml fresh cPIMDM and incubated
675 at 37°C in 5% CO2 in air.
676
677 **Enrichment of CD71 negative cRBCs**
678 Fully differentiated cRBCs were washed in degassed and chilled bead buffer (PBS + 0.5%
679 bovine serum albumin + 2mM EDTA), resuspended in the same buffer (45 µl for $6x10^6$
680 cells), and incubated the anti-CD71 antibody-immoblized beads (Miltenyi) (10µl beads for
681 $6x10^6$ cells) at 4°C for 15 min. The cells were washed in 1 ml of bead buffer and passed
682 through an LS magnetic column (Miltenyi) and washed 3 times with 2 ml of the buffer.
683 The flow through containing CD71- negative cells was collected, washed with cRPMI
684 medium and used for invasion assays.
685
686 **Detection of cell surface proteins by flow cytometry**
687 Expression of RBC surface proteins was measured in control or knockout cRBCs by flow
688 cytometry. $1x10^6$ cRBCs were washed 2 times with PBS/0.3% BSA and incubated with
689 primary monoclonal antibodies or fluorochrome conjugated antibodies at 4°C for 1 h.
690 Antibodies used: anti-CD55 (BRIC 216-PE, IBGRL; 1:50) and anti-CD71-PE (Miltenyi;
691 1:20). After incubation, the cells were washed 2 times in PBS/0.3% BSA, followed by flow
692 cytometry analysis on a MACSQuant flow cytometer (Miltenyi).
693
694 **Immunofluorecence assays (IFA)**
695 IFAs were performed as previously described, with some modifications (Tonkin et al.,
696 2004). For IFAs of CD55-CRISPR cRBCs infected with *P. falciparum*, cells were fixed in

697 4.0% paraformaldehyde and 0.0015% glutaraldehyde in PBS for 20 min at room
698 temperature and blocked for one hour in 3% BSA/PBS. The cells were incubated with
699 anti-CD55 antibody (BRIC 216-PE from IBGRL) at 1:50 concentration for 1 h at 4°C. Cells
700 were mounted Fluoromount-G with DAPI mounting medium (Electron Microscopy
701 Services) and the fluorescent images were captured with a 60X objective on a Keyence
702 BZ-X700 fluorescence microscope. For IFAs of merozoites attached to pRBCs, samples
703 were prepared as in the attachment assays (see below), and 60 ul of the samples were
704 fixed in the fixative containing 4.0% Paraformaldehyde and 0.015% Glutaraldehyde for
705 20 min, washed twice in PBS, and allowed to settle onto a Poly-L-Lysine coated coverslip
706 (Corning). The samples were then incubated in 0.1% Triton X-100/PBS for 10 min at
707 room temperature, washed in PBS, and incubated in 0.1mg/ml of NaBH4/PBS for 10 min.
708 at room temperature. Following a wash in PBS, the cells were blocked overnight in fresh
709 PBS/3.0% BSA at room temperature. Primary antibodies: mouse monoclonal Anti-
710 PfAMA1 1F9 (1:200) (Coley et al., 2001) and rabbit polyclonal anti-PfRON4 (1:200)
711 (Richard et al., 2010) were diluted in blocking buffer applied to cells for 2 hr at room
712 temperature. Following 3 washes, the cells were incubated in corresponding secondary
713 antibodies at 1:500 dilution: Alexa Fluor 555 (anti-rabbit) and Alexa Fluor 488 (anti-
714 mouse) for 1 h at room temperature. The cells were washed in PBS supplemented with
715 0.1ng/µl of DAPI (Thermofisher) and mounted in Vectashield anti-fade mounting medium.
716 Imaging was performed using a Zeiss LSM710 confocal microscope and the image
717 analysis was performed using Fiji/imageJ (Version 2.0.0-rc-69/1.52i). Apical orientation
718 was defined as PfAMA1 and PfRON4 co-localization at the cellular interface, and non-
719 apical orientation was defined as PfAMA1 and PfRON4 not co-localized at the cellular

720 interface. Merozoites were defined as being mid-invasion if AMA1 and RON4 were co-
721 localized at cellular interface and the merozoite appeared to protrude into the RBC,
722 creating an indentation.
723
724 **Anti-CD55 polyclonal antibody generation**
725 A CD55 cDNA (Asp 35-Ser 353) was cloned into a modified pTT5 vector (Raymond et
726 al., 2011), whose expression cassette consists of eGFP fused to a puromycin resistance
727 gene followed by a 2A skip peptide (Funston, Kallioinen, de Felipe, Ryan, & Iggo, 2008)
728 and a BiP signal peptide, and the resulting plasmid was verified by sequencing. 1.8L of
729 293-6E cells grown in Freestyle 293 media (Invitrogen) to 0.8x10e6 cells/ml were
730 transfected with linear PEI (Polysciences) with 397ug DNA at a 1:3 DNA:PEI
731 ratio. TN1 tryptone (Organotechnie) was added to a final concentration of 0.5% (w/v)
732 one day after transfection, and cells were grown for an additional 5 days. Cells were spun
733 down and discarded, and the following reagents were added to the harvested media (final
734 concentration listed): 20mM Tris pH8, 350mM NaCl, 5mM Imidazole pH8, 0.2mM
735 NiCl2. 6ml GE IMAC sepharose 6 beads, and the sample was rocked at 4C for 1
736 hour. The sample was then poured into a glass column, and washed with 50ml of TBS
737 (10mM Tris pH8, 500mM NaCl) with imidazole at the following concentrations
738 sequentially: 5mM, 10mM, 50mM, and 250mM. Nickel was stripped from the column with
739 10ml 100mM EDTA. The majority of the CD55-8xHis protein eluted in the 250mM
740 Imidazole fraction, with a smaller amount of equal purity in the 50mM imadazole
741 fraction. These were dialyzed separately into PBS pH 7.4 overnight at 4C, concentrated
742 to 10mg/ml using Amicon Ultra 15 with 30kDa cutoff (Millipore), snap frozen in liquid

743 nitrogen and stored at -80C until further use. 2.5 mg of CD55-8xHis was used for three
744 immunizations of two New Zealand white-SPF rabbits by New England Peptide.
745 Approximately 50ml of recovered antiserum was used for negative affinity purification with
746 an 8X HIS column, and subsequently purified with a protein A column. Approximately 15
747 ml of purified IgG at 1.209 mg/ml concentration was purified and stored at -80C
748 until further use.
749
750
751 **Live cell imaging**
752 Schizont stage *P. falciparum* strain 3D7 parasites at 4-5% parasitemia and 2% hematocrit
753 were tightly synchronized with 2 μM Compound 2 to prevent schizont rupture (Collins et
754 al., 2013). After ~4-6 hour incubation, they were washed three times and allowed to
755 recover in fresh cRPMI for 45 to 90 minutes at 37º C. After recovery, anti-CD55 antibody
756 or IgG isotype control was added to the cells at final antibody concentration of 400 μg/ml
757 and 1% hematocrit. In experiments involving previously cryopreserved CD55-null pRBCs
758 (Takahashi, 2008) or control WT pRBCs, late stage *P. falciparum* schizonts were isolated
759 using a MACS magnet, synchronized with Compound 2, and then mixed with the pRBCs
760 at 4-5% parasitemia and 1% hematocrit. The assays were loaded into a 20 mm diameter
761 Hybriwell sealing system (Grace Bio-labs) customized for live cell imaging. Rupture of the
762 parasite-infected red blood cells and subsequent invasion events were video recorded
763 using a 60X objective Keyence BZ-X700 live microscopy setup at 37°C supplied with 5%
764 CO_2 and 1% O_2 gaseous environment. For the live cell imaging of echinocytosis, 1μM
765 Cytochalasin D was added to the above mixtures. Kinetics and morphology of distinct

766 steps of invasion in the video were measured by using ImageJ (ImageJ 1.50i) as
767 described previously(Schneider et al., 2012; Weiss et al., 2015). Briefly, the following
768 events were quantified in each video: a) Contacts between merozoites and RBCs that
769 culminated in successful invasion; b) successful invasion that resulted echinocytosis; c)
770 contacts between merozoites and RBCs that could not proceed beyond initial
771 contact/deformation. d) RBCs contacted before successful invasion e) period of pre-
772 invasion (initial contact to end of deformation), f) during of internalization, g) time to the
773 onset of echinocytosis, h) efficiency and degree of merozoite-induced deformation of the
774 target RBC using a four-point deformation scale (0,1,2,3).
775
776 **Merozoite attachment assays**
777 Purified schizonts were added at 12.0% parasitemia to previously cryopreserved CD55-
778 null pRBCs (Takahashi, 2008) or control WT pRBCs at 1.0% hematocrit in the presence
779 of 1 μM Cytochalasin D, 50 U/ml Heparin or none in a final volume of 100 ul per well in a
780 96 well plate. The mixtures were incubated at 37°C for 90 min and the schizonts were
781 allowed to rupture. To quantify merozoite attachment by flow cytometry, 10 μl aliquots of
782 the samples were fixed in 2% Glutaraldehyde and 0.116M sucrose in PBS, washed in
783 PBS/0.3% BSA, and stained with SYBR Green 1 nucleic acid stain (Invitrogen). at 1:2000
784 dilution in PBS/0.3% BSA for 20 minutes, followed by flow cytometry analysis on a
785 MACSQuant flow cytometer (Miltenyi). The assays were performed 3 times with 3
786 technical replicates. The merozoite attachment rates to control or CD55-null RBCs were
787 calculated as the percent of RBCs with an attached merozoite, and were normalized for
788 background attachment in the presence of heparin. The merozoite attachment efficiency

789 was calculated for each genetic background in each biological replicate by normalizing to

790 the mean of the attachment rates in the three control experiments.

791

792 **Data analysis**

793 Stastistical analyses were performed and the graphs were generated using GraphPad Prism

794 8 Version 8.0.2 (159) for macOS.

795
796

797 **Supplemental Information**
798 Supplemental information includes six figures and eight movies.

799

800 **Multimedia Files**

801 Movie S1: *P. falciparum* 3D7 invasion in the presence of isotype control antibody.

802 Movie S2: *P. falciparum* 3D7 invasion in the presence of anti-CD55 antibody.

803 Movie S3: *P. falciparum* 3D7 merozoite-induced deformation with deformation score 1.

804 Movie S4: *P. falciparum* 3D7 merozoite-induced deformation with deformation score 2.

805 Movie S5: *P. falciparum* 3D7 merozoite-induced deformation with deformation score 3.

806 Movie S6: An example of a failed invasion despite successful merozoite-induced
807 deformation in CD55-null pRBC.

808 Movie S7: An example of a successful invasion of a wild-type pRBC.

809 Movie S8: Echinocytosis induced by attached *P. falciparum* merozoite to pRBCs in the
810 presence of Cytochalasin D. Black arrows: Attachment resulting echinocyte formation.
811 White arrows: Attachment resulting no echinocyte formation.

812

813

814

References

Alexander, D. L., Arastu-Kapur, S., Dubremetz, J. F., & Boothroyd, J. C. (2006). *Plasmodium falciparum* AMA1 binds a rhoptry neck protein homologous to TgRON4, a component of the moving junction in *Toxoplasma gondii*. *Eukaryot Cell, 5*(7), 1169-1173. doi:10.1128/EC.00040-06

Alexander, D. L., Mital, J., Ward, G. E., Bradley, P., & Boothroyd, J. C. (2005). Identification of the moving junction complex of *Toxoplasma gondii*: a collaboration between distinct secretory organelles. *PLoS Pathog, 1*(2), e17. doi:10.1371/journal.ppat.0010017

Bei, A. K., & Duraisingh, M. T. (2012). Functional analysis of erythrocyte determinants of *Plasmodium infection*. *Int J Parasitol, 42*(6), 575-582. doi:10.1016/j.ijpara.2012.03.006

Besteiro, S., Dubremetz, J. F., & Lebrun, M. (2011). The moving junction of apicomplexan parasites: a key structure for invasion. *Cell Microbiol, 13*(6), 797-805. doi:10.1111/j.1462-5822.2011.01597.x

Besteiro, S., Michelin, A., Poncet, J., Dubremetz, J. F., & Lebrun, M. (2009). Export of a *Toxoplasma gondii* rhoptry neck protein complex at the host cell membrane to form the moving junction during invasion. *PLoS Pathog, 5*(2), e1000309. doi:10.1371/journal.ppat.1000309

Chen, L., Lopaticki, S., Riglar, D. T., Dekiwadia, C., Uboldi, A. D., Tham, W. H., . . . Cowman, A. F. (2011). An EGF-like protein forms a complex with PfRh5 and is required for invasion of human erythrocytes by *Plasmodium falciparum*. *PLoS Pathog, 7*(9), e1002199. doi:10.1371/journal.ppat.1002199

Chu, T. T. T., Sinha, A., Malleret, B., Suwanarusk, R., Park, J. E., Naidu, R., . . . Chandramohanadas, R. (2018). Quantitative mass spectrometry of human reticulocytes reveal proteome-wide modifications during maturation. *Br J Haematol, 180*(1), 118-133. doi:10.1111/bjh.14976

Coley, A. M., Campanale, N. V., Casey, J. L., Hodder, A. N., Crewther, P. E., Anders, R. F., . . . Foley, M. (2001). Rapid and precise epitope mapping of monoclonal antibodies against *Plasmodium falciparum* AMA1 by combined phage display of fragments and random peptides. *Protein Eng, 14*(9), 691-698. doi:10.1093/protein/14.9.691

Collins, C. R., Hackett, F., Strath, M., Penzo, M., Withers-Martinez, C., Baker, D. A., & Blackman, M. J. (2013). Malaria parasite cGMP-dependent protein kinase regulates blood stage merozoite secretory organelle discharge and egress. *PLoS Pathog, 9*(5), e1003344. doi:10.1371/journal.ppat.1003344

858 Cooling, L. (2015). Blood Groups in Infection and Host Susceptibility. *Clin Microbiol Rev, 28*(3),
859 801-870. doi:10.1128/CMR.00109-14
860
861 Coyne, C. B., & Bergelson, J. M. (2006). Virus-induced Abl and Fyn kinase signals permit
862 coxsackievirus entry through epithelial tight junctions. *Cell, 124*(1), 119-131.
863 doi:10.1016/j.cell.2005.10.035
864
865 Crosnier, C., Bustamante, L. Y., Bartholdson, S. J., Bei, A. K., Theron, M., Uchikawa, M., . . .
866 Wright, G. J. (2012). Basigin is a receptor essential for erythrocyte invasion by
867 *Plasmodium falciparum*. *Nature, 480*(7378), 534-537. doi:nature10606 [pii]
868 10.1038/nature10606
869
870 Dreyer, A. M., Matile, H., Papastogiannidis, P., Kamber, J., Favuzza, P., Voss, T. S., . . . Pluschke,
871 G. (2012). Passive immunoprotection of *Plasmodium falciparum*-infected mice
872 designates the CyRPA as candidate malaria vaccine antigen. *J Immunol, 188*(12), 6225-
873 6237. doi:10.4049/jimmunol.1103177
874
875 Dvorak, J. A., Miller, L. H., Whitehouse, W. C., & Shiroishi, T. (1975). Invasion of erythrocytes by
876 malaria merozoites. *Science, 187*(4178), 748-750. doi:10.1126/science.803712
877
878 Egan, E. S. (2017). Beyond Hemoglobin: Screening for Malaria Host Factors. *Trends Genet*.
879 doi:10.1016/j.tig.2017.11.004
880
881 Egan, E. S., Jiang, R. H., Moechtar, M. A., Barteneva, N. S., Weekes, M. P., Nobre, L. V., . . .
882 Duraisingh, M. T. (2015). Malaria. A forward genetic screen identifies erythrocyte CD55
883 as essential for *Plasmodium falciparum* invasion. *Science, 348*(6235), 711-714.
884 doi:10.1126/science.aaa3526
885
886 Funston, G. M., Kallioinen, S. E., de Felipe, P., Ryan, M. D., & Iggo, R. D. (2008). Expression of
887 heterologous genes in oncolytic adenoviruses using picornaviral 2A sequences that
888 trigger ribosome skipping. *J Gen Virol, 89*(Pt 2), 389-396. doi:10.1099/vir.0.83444-0
889
890 Gautier, E. F., Ducamp, S., Leduc, M., Salnot, V., Guillonneau, F., Dussiot, M., . . . Mayeux, P.
891 (2016). Comprehensive Proteomic Analysis of Human Erythropoiesis. *Cell Rep, 16*(5),
892 1470-1484. doi:10.1016/j.celrep.2016.06.085
893
894 Giarratana, M. C., Kobari, L., Lapillonne, H., Chalmers, D., Kiger, L., Cynober, T., . . . Douay, L.
895 (2005). Ex vivo generation of fully mature human red blood cells from hematopoietic
896 stem cells. *Nat Biotechnol, 23*(1), 69-74. doi:nbt1047 [pii]10.1038/nbt1047
897
898 Giarratana, M. C., Rouard, H., Dumont, A., Kiger, L., Safeukui, I., Le Pennec, P. Y., . . . Douay, L.
899 (2011). Proof of principle for transfusion of in vitro-generated red blood cells. *Blood,*
900 *118*(19), 5071-5079. doi:blood-2011-06-362038 [pii] 10.1182/blood-2011-06-362038
901

902 Gilson, P. R., & Crabb, B. S. (2009). Morphology and kinetics of the three distinct phases of red
903 blood cell invasion by *Plasmodium falciparum* merozoites. *Int J Parasitol, 39*(1), 91-96.
904 doi:10.1016/j.ijpara.2008.09.007
905
906 Harvey, K. L., Yap, A., Gilson, P. R., Cowman, A. F., & Crabb, B. S. (2014). Insights and
907 controversies into the role of the key apicomplexan invasion ligand, Apical Membrane
908 Antigen 1. *Int J Parasitol, 44*(12), 853-857. doi:10.1016/j.ijpara.2014.08.001
909
910 Hendel, A., Bak, R. O., Clark, J. T., Kennedy, A. B., Ryan, D. E., Roy, S., . . . Porteus, M. H. (2015).
911 Chemically modified guide RNAs enhance CRISPR-Cas genome editing in human primary
912 cells. *Nat Biotechnol, 33*(9), 985-989. doi:10.1038/nbt.3290
913
914 Hu, G., Cabrera, A., Kono, M., Mok, S., Chaal, B. K., Haase, S., . . . Bozdech, Z. Transcriptional
915 profiling of growth perturbations of the human malaria parasite *Plasmodium falciparum*.
916 *Nat Biotechnol, 28*(1), 91-98. doi:nbt.1597 [pii] 10.1038/nbt.1597
917
918 Hu, J., Liu, J., Xue, F., Halverson, G., Reid, M., Guo, A., . . . An, X. (2013). Isolation and functional
919 characterization of human erythroblasts at distinct stages: implications for
920 understanding of normal and disordered erythropoiesis in vivo. *Blood, 121*(16), 3246-
921 3253. doi:10.1182/blood-2013-01-476390
922
923 Kanjee, U., Gruring, C., Chaand, M., Lin, K. M., Egan, E., Manzo, J., . . . Duraisingh, M. T. (2017).
924 CRISPR/Cas9 knockouts reveal genetic interaction between strain-transcendent
925 erythrocyte determinants of *Plasmodium falciparum* invasion. *Proc Natl Acad Sci U S A,*
926 *114*(44), E9356-E9365. doi:10.1073/pnas.1711310114
927
928 Koch, M., & Baum, J. (2016). The mechanics of malaria parasite invasion of the human
929 erythrocyte - towards a reassessment of the host cell contribution. *Cell Microbiol, 18*(3),
930 319-329. doi:10.1111/cmi.12557
931
932 Malleret, B., Xu, F., Mohandas, N., Suwanarusk, R., Chu, C., Leite, J. A., . . . Russell, B. (2013).
933 Significant biochemical, biophysical and metabolic diversity in circulating human cord
934 blood reticulocytes. *PLoS One, 8*(10), e76062. doi:10.1371/journal.pone.0076062
935
936 Miller, L. H., Aikawa, M., Johnson, J. G., & Shiroishi, T. (1979). Interaction between cytochalasin
937 B-treated malarial parasites and erythrocytes. Attachment and junction formation. *J Exp*
938 *Med, 149*(1), 172-184.
939
940 Ord, R. L., Rodriguez, M., & Lobo, C. A. (2015). Malaria invasion ligand RH5 and its prime
941 candidacy in blood-stage malaria vaccine design. *Hum Vaccin Immunother, 11*(6), 1465-
942 1473. doi:10.1080/21645515.2015.1026496
943

944 Pasvol, G., Chasis, J. A., Mohandas, N., Anstee, D. J., Tanner, M. J., & Merry, A. H. (1989).
945 Inhibition of malarial parasite invasion by monoclonal antibodies against glycophorin A
946 correlates with reduction in red cell membrane deformability. *Blood, 74*(5), 1836-1843.
947
948 Paul, A. S., Egan, E. S., & Duraisingh, M. T. (2015). Host-parasite interactions that guide red
949 blood cell invasion by malaria parasites. *Curr Opin Hematol, 22*(3), 220-226.
950 doi:10.1097/MOH.0000000000000135
951
952 Raymond, C., Tom, R., Perret, S., Moussouami, P., L'Abbe, D., St-Laurent, G., & Durocher, Y.
953 (2011). A simplified polyethylenimine-mediated transfection process for large-scale and
954 high-throughput applications. *Methods, 55*(1), 44-51. doi:10.1016/j.ymeth.2011.04.002
955
956 Reddy, K. S., Amlabu, E., Pandey, A. K., Mitra, P., Chauhan, V. S., & Gaur, D. (2015). Multiprotein
957 complex between the GPI-anchored CyRPA with PfRH5 and PfRipr is crucial for
958 *Plasmodium falciparum* erythrocyte invasion. *Proc Natl Acad Sci U S A, 112*(4), 1179-
959 1184. doi:10.1073/pnas.1415466112
960
961 Richard, D., MacRaild, C. A., Riglar, D. T., Chan, J. A., Foley, M., Baum, J., . . . Cowman, A. F.
962 (2010). Interaction between *Plasmodium falciparum* apical membrane antigen 1 and the
963 rhoptry neck protein complex defines a key step in the erythrocyte invasion process of
964 malaria parasites. *J Biol Chem, 285*(19), 14815-14822. doi:10.1074/jbc.M109.080770
965
966 Riglar, D. T., Richard, D., Wilson, D. W., Boyle, M. J., Dekiwadia, C., Turnbull, L., . . . Baum, J.
967 (2011). Super-resolution dissection of coordinated events during malaria parasite
968 invasion of the human erythrocyte. *Cell Host Microbe, 9*(1), 9-20.
969 doi:10.1016/j.chom.2010.12.003
970
971 Sack, B., Kappe, S. H., & Sather, D. N. (2017). Towards functional antibody-based vaccines to
972 prevent pre-erythrocytic malaria infection. *Expert Rev Vaccines, 16*(5), 403-414.
973 doi:10.1080/14760584.2017.1295853
974
975 Salinas, N. D., Tang, W. K., & Tolia, N. H. (2019). Blood-Stage Malaria Parasite Antigens:
976 Structure, Function, and Vaccine Potential. *J Mol Biol, 431*(21), 4259-4280.
977 doi:10.1016/j.jmb.2019.05.018
978
979 Satchwell, T. J., Wright, K. E., Haydn-Smith, K. L., Sanchez-Roman Teran, F., Moura, P. L.,
980 Hawksworth, J., . . . Baum, J. (2019). Genetic manipulation of cell line derived
981 reticulocytes enables dissection of host malaria invasion requirements. *Nat Commun,*
982 *10*(1), 3806. doi:10.1038/s41467-019-11790-w
983
984 Schneider, C. A., Rasband, W. S., & Eliceiri, K. W. (2012). NIH Image to ImageJ: 25 years of Image
985 Analysis. *Nature Methods, 9*(7), 671-675.
986

987 Scully, E. J., Shabani, E., Rangel, G. W., Gruring, C., Kanjee, U., Clark, M. A., . . . Duraisingh, M. T.
988 (2019). Generation of an immortalized erythroid progenitor cell line from peripheral
989 blood: A model system for the functional analysis of *Plasmodium* spp. invasion. *Am J*
990 *Hematol, 94*(9), 963-974. doi:10.1002/ajh.25543
991
992 Spadafora, C., Awandare, G. A., Kopydlowski, K. M., Czege, J., Moch, J. K., Finberg, R. W., . . .
993 Stoute, J. A. (2010). Complement receptor 1 is a sialic acid-independent erythrocyte
994 receptor of *Plasmodium falciparum*. *PLoS Pathog, 6*(6), e1000968.
995 doi:10.1371/journal.ppat.1000968
996
997 Srinivasan, P., Beatty, W. L., Diouf, A., Herrera, R., Ambroggio, X., Moch, J. K., . . . Miller, L. H.
998 (2011). Binding of *Plasmodium* merozoite proteins RON2 and AMA1 triggers
999 commitment to invasion. *Proc Natl Acad Sci U S A, 108*(32), 13275-13280.
1000 doi:10.1073/pnas.1110303108
1001
1002 Storry, J. R., Reid, M. E., & Yazer, M. H. (2010). The Cromer blood group system: a review.
1003 *Immunohematology, 26*(3), 109-118.
1004
1005 Takahashi, J. Y. S., Yamane S, Tanaka M, Takahashi H, et al. (2008). A case of Inab phenotype
1006 (IFC-) with anti-IFC. *Jpn J Transfusion and Cell Therapy, 54*(2), 258.
1007
1008 Taylor, S. M., & Fairhurst, R. M. (2014). Malaria parasites and red cell variants: when a house is
1009 not a home. *Curr Opin Hematol, 21*(3), 193-200. doi:10.1097/MOH.0000000000000039
1010
1011 Tham, W. H., Healer, J., & Cowman, A. F. (2012). Erythrocyte and reticulocyte binding-like
1012 proteins of *Plasmodium falciparum*. *Trends Parasitol, 28*(1), 23-30.
1013 doi:10.1016/j.pt.2011.10.002
1014
1015 Tiffert, T., Lew, V. L., Ginsburg, H., Krugliak, M., Croisille, L., & Mohandas, N. (2005). The
1016 hydration state of human red blood cells and their susceptibility to invasion by
1017 *Plasmodium falciparum*. *Blood, 105*(12), 4853-4860. doi:10.1182/blood-2004-12-4948
1018
1019 Tonkin, C. J., van Dooren, G. G., Spurck, T. P., Struck, N. S., Good, R. T., Handman, E., . . .
1020 McFadden, G. I. (2004). Localization of organellar proteins in Plasmodium falciparum
1021 using a novel set of transfection vectors and a new immunofluorescence fixation
1022 method. *Mol Biochem Parasitol, 137*(1), 13-21. doi:10.1016/j.molbiopara.2004.05.009
1023
1024 Volz, J. C., Yap, A., Sisquella, X., Thompson, J. K., Lim, N. T., Whitehead, L. W., . . . Cowman, A. F.
1025 (2016). Essential Role of the PfRh5/PfRipr/CyRPA Complex during *Plasmodium*
1026 *falciparum* Invasion of Erythrocytes. *Cell Host Microbe, 20*(1), 60-71.
1027 doi:10.1016/j.chom.2016.06.004
1028
1029 Weiss, G. E., Gilson, P. R., Taechalertpaisarn, T., Tham, W. H., de Jong, N. W., Harvey, K. L., . . .
1030 Crabb, B. S. (2015). Revealing the Sequence and Resulting Cellular Morphology of

1031 Receptor-Ligand Interactions during *Plasmodium falciparum* Invasion of Erythrocytes.
1032 *PLoS Pathog, 11*(2), e1004670. doi:10.1371/journal.ppat.1004670
1033
1034 WHO. (2018). *World Malaria Report 2018*. World Health Organization, Geneva.
1035
1036 Yap, A., Azevedo, M. F., Gilson, P. R., Weiss, G. E., O'Neill, M. T., Wilson, D. W., . . . Cowman, A.
1037 F. (2014). Conditional expression of apical membrane antigen 1 in *Plasmodium*
1038 *falciparum* shows it is required for erythrocyte invasion by merozoites. *Cell Microbiol,*
1039 *16*(5), 642-656. doi:10.1111/cmi.12287
1040